Northumbria Research Link

Article

Saturated-Phase Densities of (CO$_2$ + Methylcyclohexane) at Temperatures from 298 to 448 K and Pressures up to the Critical Pressure

Yolanda Sanchez-Vicente* and J. P. Martin Trusler

Read Online

| ACCESS | | 📊 Metrics & More | | 📰 Article Recommendations |

ABSTRACT: This work reports saturated-phase densities for the CO$_2$ + methylcyclohexane system at temperatures between 298 and 448 K and at pressures up to the critical pressure. The densities were measured with a standard uncertainty of <1.5 kg·m^{-3} and were fitted along isotherms with a recently developed nonlinear empirical correlation with an absolute average deviation (Δ_{AAD}) of about 1.5 kg·m^{-3}. This empirical correlation also allowed the estimation of the critical pressure and density at each temperature, and the obtained critical pressures were found to be in close agreement with previously published data. We also compare both our density data and vapor−liquid equilibrium (VLE) data from the literature with the predictions from two models: PPR-78 and SAFT-γ Mie. The results show that densities

were predicted better with SAFT-γ Mie than with PPR-78, whereas PPR-78 generally performed better for VLE. This could indicate that some of the unlike parameters of SAFT-γ Mie could be further optimized.
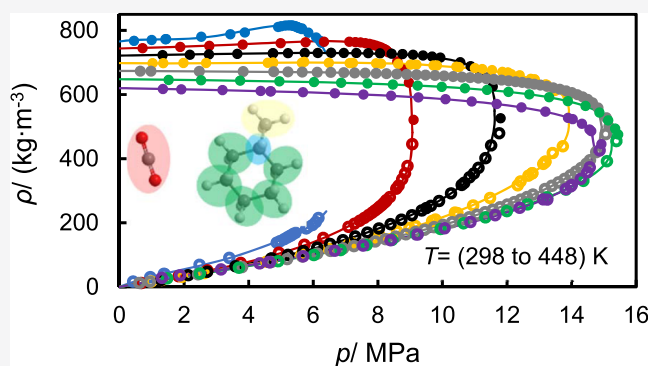
1. INTRODUCTION

Mixtures of carbon dioxide and hydrocarbons are involved in many industrial applications such as supercritical extraction,[1] separation processes,[2,3] gas hydrates applications,[4] and carbon capture and storage (CCS).[5] The thermophysical properties of (CO$_2$ + hydrocarbon) systems over wide ranges of pressures and temperatures are necessary to design and optimize the aforementioned processes.[6] For instance, in CCS, the CO$_2$ storage capacity on an oil reservoir is affected, in part, by the density and phase behavior of such mixtures. Convective flows within the reservoir also depend upon the density difference between the vapor and liquid phases.[7] Furthermore, thermodynamic models employed in the simulation process must be evaluated against reliable experimental data to achieve the optimal design and operation of the industrial application.

Recently, predictive thermodynamic models have been developed that cover wide ranges of both operation conditions and chemical components. Jaubert and co-workers developed the predictive Peng−Robinson equation (PPR-78).[8−10] PPR-78 uses a group-contribution approach based on the type and number of functional groups existing in each component to predict the binary interaction parameters between unlike molecules as functions of temperatures. The PPR-78 model was successfully used to describe the fluid phase behavior of mixtures that contained paraffin, naphthenes, aromatics, and CO$_2$.[11,12] Another group-contribution approach is the SAFT-γ

Mie model,[13−15] a molecular method based on the statistical associating fluid theory (SAFT). In SAFT-γ Mie, the molecules are represented as different functional groups using a fused heteronuclear model. The Mie potential is adopted to represent the group−group interactions. A number of like and unlike parameters are employed to describe the interactions of the functional groups and are determined by regression of experimental properties for pure components and binary mixtures. The most recent version of SAFT-γ Mie contains 58 functional groups, including, among others, those required to describe aromatic and cyclic compounds, and CO$_2$.[16] It has been used to describe the phase behavior and thermodynamic properties of multiple systems.

To assist in developing thermodynamic models, we have investigated the thermophysical properties of several (CO$_2$ + hydrocarbon) systems over wide pressure and temperature ranges. Specifically, our group has reported densities and vapor−liquid equilibrium (VLE) data for the systems (CO$_2$ + *n*-heptane) and (CO$_2$ + methylbenzene), both mixtures involving

Table 1. Description of Chemicals Where x and w Denote the Mole Fraction and Mass Fraction, Respectively[a]

chemical name	CAS number	source	purity as supplied	additional purification
water	7732-18-5	Millipore Direct Q UV3	$\rho_{elec} > 18$ MΩ·cm	degassed under vacuum
carbon dioxide	124-38-9	BOC	$x \geq 0.99995$	none
methylcyclohexane	108-87-2	Sigma-Aldrich	$w \geq 0.99$	degassed under vacuum

[a] ρ_{elec} denotes electrical resistivity at $T = 298.15$ K.
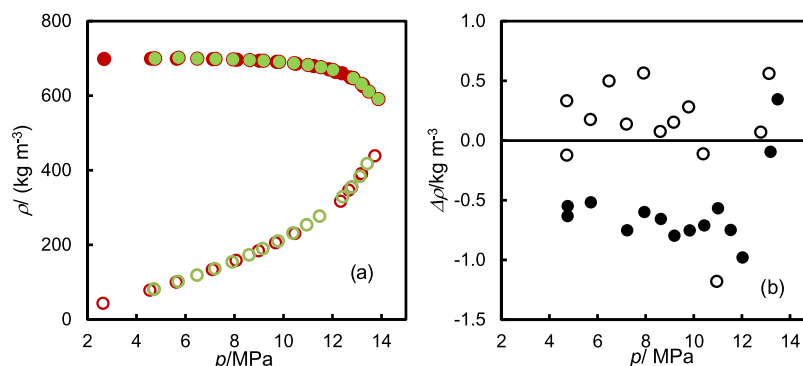
Figure 1. (a) Saturated-phase densities for the CO_2 + methylcyclohexane system as a function of pressure at 373 K measured at different times: green circles, first measurement, and red circles, second measurement. (b) Differences between the saturated-phase densities measured in the first and second places. Dew-point densities are represented by open symbols, whereas solid symbols represent bubble-point densities.

a hydrocarbon containing seven carbon atoms.[17−20] In this paper, we present the saturated-phase densities for another system of that type: (CO_2 + methylcyclohexane). Several authors have reported VLE data for this system. Field et al.[21] measured the solubility of CO_2 in methylcyclohexane at atmospheric pressures and in a temperature range from 283 to 313 K. Ng and Robinson[22] used an analytical apparatus to measure the VLE from 310 to 478 K up to the critical pressure, and they fitted the data with the Peng−Robinson equation of state.[23] Later, Peters and co-workers determined bubble points at temperatures from 263 to 353 K and at pressures from 0.4 to 11.5 MPa.[24,25] Critical points have also been measured from 304 to 477 K by several authors.[22,26] However, to date, density data have not been reported for this system. The present work addresses this gap in the literature by reporting saturated-phase densities at temperatures from 298 to 448 K at pressures up to the critical locus. We performed these measurements using a custom-built apparatus.[27] An empirical equation has been applied to correlate the density data along isotherms to within the experimental uncertainty. Finally, we evaluate the predictive capabilities of PPR-78 and SAFT-γ Mie with respect to saturated-phase densities and compositions.

2. MATERIALS AND METHODS

2.1. Materials. Table 1 describes the chemicals employed in this study. Methylcyclohexane and water were degassed briefly under vacuum before injecting into the apparatus. No other analysis or purification was attempted.

2.2. Saturated-Phase Density Measurement. A comprehensive description of the apparatus can be found in our previous work.[27] In brief, the experimental setup included two vibrating-tube densimeters (VTD, Anton Paar, DMA-HP), an equilibrium cell, and two syringe pumps. The equilibrium cell and the two densimeters were placed inside a thermostatically controlled oven with an operating range of 293−473 K and uniformity and stability of ±0.2 K. The top and bottom parts of the equilibrium cell were linked to the two VTDs. A coiled tube with a volume of 6 mL connected each densimeter to a syringe
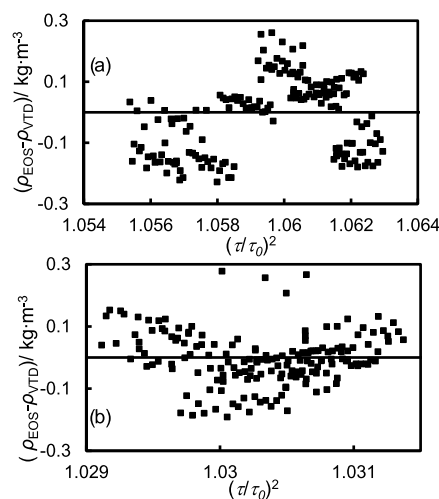
Figure 2. Difference between water densities calculated the IAPWS[30] and the VTD densities for (a) top densimeter and (b) bottom densimeter.

pump (Quizix model C-5000-10K). A calibrated pressure transducer (Sensata Technology, model 101HP2) was attached to each pump cylinder to monitor the pressure. The temperature of the two VTDs and the equilibrium cell was all measured using Pt100 thermometers. The maximum working pressure of the apparatus was 70 MPa at temperatures up to 473.15 K.

The experimental procedure was as follows. The apparatus was first emptied and flushed with CO_2 several times. Next, methylcyclohexane was pumped into the equilibrium cell through the bottom VTD until roughly half of the cell capacity was filled. After that, CO_2 was injected into the cell to reach the desired pressure, and the mixture was agitated while maintaining the set pressure with the CO_2 pump in a constant pressure mode. Once equilibrium was achieved (as judged by the constancy of temperature, pressure, and CO_2 pump volume), 4 mL of the liquid phase was displaced into the bottom VTD by slowly retracting the bottom syringe pump, while the top pump,

Table 2. Experimental Saturated Densities ρ for the CO_2 + Methylcyclohexane System at Temperatures T and Pressures $p^{a,b}$

	liquid phase				vapor phase		
T/K	p/MPa	$\rho/(kg\cdot m^{-3})$	$u(\rho)/(kg\cdot m^{-3})$	T/K	p/MPa	$\rho/(kg\cdot m^{-3})$	$u(\rho)/(kg\cdot m^{-3})$
297.7	0.45	767.4	0.4	297.7	0.43	16.5	1.6
297.7	0.99	770.3	0.2	297.7	0.95	30.1	1.3
297.8	1.42	772.6	0.2	297.8	1.38	40.4	1.2
297.7	1.44	772.8	0.2	297.8	1.40	40.2	1.1
297.9	2.53	780.3	0.5	297.9	2.48	68.5	1.2
297.9	3.43	787.9	1.0	297.9	3.40	90.5	1.5
297.9	3.88	793.5	1.0	297.8	4.87	137.5	2.0
297.9	4.91	810.5	0.5	297.8	4.98	142.4	2.0
297.8	5.01	813.0	0.4	297.7	5.10	148.7	2.1
297.8	5.13	815.2	0.5	297.7	5.20	154.1	2.2
297.8	5.24	815.9	0.6	297.7	5.28	158.6	2.2
297.8	5.32	815.6	0.8	297.7	5.34	161.8	2.3
297.8	5.37	814.7	0.9	297.7	5.39	164.7	2.3
297.8	5.41	813.5	1.1	297.7	5.43	167.1	2.3
297.8	5.45	812.2	1.2	297.7	5.46	169.0	2.4
297.8	5.48	810.8	1.3	298.0	5.78	182.0	2.9
297.8	5.53	809.5	1.4	298.0	5.83	185.5	3.0
297.8	5.55	808.1	1.5	298.0	5.98	192.5	3.5
297.8	5.56	807.4	1.6	298.0	6.08	202.2	3.9
298.0	5.64	803.9	2.0	297.9	6.16	215.0	4.4
297.9	5.65	806.1	2.0	322.8	0.68	11.8	0.9
298.1	5.85	792.8	3.1	322.8	1.83	33.1	0.9
298.1	6.09	778.0	5.2	322.8	2.72	51.3	1.0
298.2	6.20	768.0	6.7	322.8	3.76	74.8	1.2
298.1	6.26	761.3	7.5	322.8	4.94	106.3	1.5
322.9	0.71	744.8	0.2	322.8	5.73	131.3	1.8
322.9	1.88	748.6	0.3	322.8	6.31	152.7	2.1
322.9	2.78	751.7	0.3	322.8	7.09	187.3	2.7
322.9	3.82	755.6	0.3	322.8	7.28	197.2	2.9
322.9	4.99	760.1	0.3	322.8	7.44	206.2	3.1
322.9	5.76	763.0	0.3	322.8	7.58	214.9	3.3
322.8	6.33	764.7	0.3	322.8	7.71	223.2	3.5
322.9	7.12	764.5	0.5	322.8	7.81	230.5	3.6
322.9	7.31	763.6	0.6	322.8	7.91	237.6	3.8
322.9	7.47	762.1	0.8	322.8	7.99	243.9	4.0
322.9	7.61	760.2	1.0	322.8	8.06	249.7	4.2
322.9	7.74	757.9	1.2	322.8	8.12	255.2	4.3
322.9	7.84	755.3	1.4	322.8	8.18	259.9	4.5
322.9	7.94	752.4	1.6	322.8	8.22	264.4	4.6
322.9	8.02	749.6	1.9	322.8	8.26	267.9	4.8
322.9	8.09	746.8	2.1	322.8	8.27	270.3	4.8
322.9	8.15	743.8	2.3	322.8	8.37	280.0	5.2
322.9	8.21	741.0	2.5	322.8	8.57	305.8	6.4
322.9	8.25	738.3	2.7	322.7	8.64	315.5	7.0
322.9	8.29	735.2	2.9	322.8	8.75	335.6	8.5
322.9	8.32	732.0	3.1	322.8	8.84	353.7	10.4
322.9	8.60	703.6	5.5	322.8	8.92	376.8	13.6
322.9	8.79	677.9	9.2	322.8	9.07	445.1	15.4
322.9	8.96	637.5	20.7	347.8	1.29	21.5	0.8
322.9	9.10	521.0	20.7	347.8	2.13	36.2	0.9
348.0	1.33	722.6	0.2	347.8	2.72	47.1	0.9
348.0	2.18	724.2	0.2	347.8	3.59	64.2	1.0
348.0	2.77	725.3	0.2	347.8	4.70	88.0	1.1
348.0	3.65	726.6	0.2	347.8	4.71	88.4	1.1
348.0	4.74	728.3	0.2	347.8	5.22	100.0	1.2
348.0	4.76	728.3	0.2	347.8	5.70	111.7	1.3
348.0	5.21	728.9	0.2	347.8	6.12	122.8	1.4
348.0	5.74	729.4	0.2	347.8	6.52	133.8	1.4
348.0	6.14	729.7	0.2	347.8	6.92	145.3	1.5

Table 2. continued

	liquid phase				vapor phase		
T/K	p/MPa	$\rho/(\text{kg}\cdot\text{m}^{-3})$	$u(\rho)/(\text{kg}\cdot\text{m}^{-3})$	T/K	p/MPa	$\rho/(\text{kg}\cdot\text{m}^{-3})$	$u(\rho)/(\text{kg}\cdot\text{m}^{-3})$
348.0	6.55	729.9	0.2	347.8	7.30	157.1	1.6
348.0	6.95	729.8	0.2	347.8	7.68	169.4	1.7
348.0	7.33	729.6	0.3	347.8	8.04	182.0	1.9
348.0	7.70	729.2	0.3	347.8	8.40	195.5	2.0
348.0	8.07	728.5	0.3	347.8	8.73	209.2	2.2
348.0	8.42	727.5	0.3	347.8	9.06	223.4	2.3
348.0	8.76	726.0	0.4	347.8	9.36	238.0	2.5
348.0	9.09	724.1	0.4	347.8	9.50	245.4	2.6
348.0	9.40	721.6	0.5	347.8	9.64	252.8	2.7
348.0	9.68	718.5	0.6	347.8	9.90	267.9	3.0
348.0	9.93	714.9	0.8	347.8	10.26	291.8	3.5
348.0	10.55	700.5	1.4	347.8	10.60	317.6	4.1
348.0	10.87	688.7	2.2	347.8	10.68	324.7	4.3
348.0	11.15	673.1	3.5	347.9	10.84	341.9	4.9
348.0	11.38	653.0	6.3	347.8	10.98	353.5	5.5
348.0	11.56	625.3	19.3	347.8	11.12	371.3	6.4
348.0	11.80	525.8	19.3	347.8	11.33	401.2	9.1
373.1	1.02	697.9	0.2	347.8	11.51	441.0	9.1
373.3	1.35	697.6	0.2	347.8	11.76	478.8	9.3
373.1	1.98	698.7	0.2	373.0	0.98	16.3	0.9
373.3	2.68	698.5	0.2	373.1	1.31	21.6	0.9
373.3	4.59	699.1	0.2	372.9	1.94	31.5	0.8
373.2	4.75	699.7	0.2	373.1	2.63	43.2	0.8
373.2	4.76	699.6	0.2	373.1	4.55	78.1	0.9
373.3	5.65	699.0	0.2	373.0	4.72	81.0	0.9
373.2	5.72	701.6	0.2	373.0	4.72	81.3	0.9
373.2	6.48	699.1	0.2	373.1	5.63	99.9	1.0
373.3	7.12	697.9	0.3	373.0	5.70	101.5	1.0
373.2	7.23	698.3	0.3	373.0	6.47	118.6	1.1
373.2	7.94	697.1	0.3	373.1	7.10	133.3	1.2
373.4	8.10	696.2	0.3	373.0	7.20	135.8	1.2
373.1	8.63	695.5	0.3	373.0	7.91	154.0	1.3
373.3	9.01	693.6	0.3	373.1	8.07	158.1	1.4
373.1	9.19	693.6	0.3	372.9	8.60	173.0	1.5
373.3	9.72	690.6	0.4	373.1	8.98	184.1	1.6
373.1	9.83	690.7	0.4	372.9	9.16	189.7	1.6
373.1	10.43	687.0	0.5	373.1	9.68	205.4	1.8
373.3	10.52	685.7	0.5	372.9	9.78	209.9	1.8
373.1	11.00	682.1	0.6	372.9	10.39	231.4	2.0
373.3	11.23	679.3	0.7	373.1	10.47	230.2	2.0
373.1	11.53	676.1	0.8	372.9	10.95	253.7	2.2
373.3	11.85	670.6	0.9	372.9	11.47	277.0	2.5
373.1	12.02	668.8	1.0	373.1	12.33	316.8	3.0
373.3	12.13	663.5	1.0	372.9	12.42	328.8	3.1
373.3	12.39	660.1	1.2	373.1	12.67	346.6	3.4
373.3	12.74	648.7	1.5	372.9	12.78	354.2	3.5
373.1	12.85	647.1	1.6	373.1	12.79	354.7	3.5
373.3	12.86	646.9	1.6	372.9	13.12	383.4	4.1
373.1	13.19	631.5	2.2	373.1	13.18	389.3	4.3
373.3	13.24	629.8	2.3	373.1	13.19	390.8	4.3
373.3	13.26	625.6	2.3	372.9	13.42	417.6	5.1
373.1	13.48	611.0	3.2	373.1	13.73	438.7	5.2
373.1	13.88	590.9	3.3	398.2	0.62	12.0	0.8
398.4	0.64	672.6	0.2	398.2	0.94	16.6	0.8
398.4	0.98	672.5	0.2	398.2	2.43	39.3	0.8
398.4	2.47	672.3	0.2	398.2	3.79	61.5	0.9
398.4	3.83	671.6	0.2	398.2	4.70	77.3	0.9
398.4	4.78	670.9	0.2	398.2	5.19	86.2	0.9
398.5	5.22	670.5	0.2	398.2	5.66	95.1	0.9

Table 2. continued

liquid phase				vapor phase			
T/K	p/MPa	ρ/(kg·m⁻³)	u(ρ)/(kg·m⁻³)	T/K	p/MPa	ρ/(kg·m⁻³)	u(ρ)/(kg·m⁻³)
398.5	5.66	670.0	0.2	398.2	6.13	103.9	1.0
398.4	6.13	669.4	0.3	398.2	6.53	112.0	1.0
398.4	6.54	668.7	0.3	398.2	6.92	120.0	1.0
398.4	6.95	668.0	0.3	398.2	7.26	127.1	1.1
398.4	7.28	667.3	0.3	398.1	7.59	134.1	1.1
398.4	7.61	666.6	0.3	398.2	7.92	141.5	1.1
398.4	7.94	665.7	0.3	398.2	8.24	148.8	1.2
398.4	8.27	664.8	0.3	398.1	8.56	156.3	1.2
398.4	8.59	663.8	0.3	398.1	8.87	163.9	1.2
398.4	8.90	662.8	0.3	398.2	9.17	171.3	1.3
398.4	9.20	661.6	0.3	398.2	9.45	178.3	1.3
398.4	9.48	660.4	0.3	398.2	9.74	186.1	1.3
398.4	9.77	659.0	0.4	398.2	10.02	193.5	1.4
398.4	10.05	657.7	0.4	398.2	10.30	201.5	1.4
398.4	10.33	656.1	0.4	398.2	10.57	209.2	1.5
398.4	10.60	654.5	0.4	398.2	10.83	217.1	1.5
398.4	10.86	652.7	0.4	398.2	11.08	224.8	1.6
398.4	11.11	651.0	0.5	398.2	11.32	232.7	1.6
398.4	11.36	649.0	0.5	398.2	11.56	240.7	1.7
398.4	11.60	646.9	0.5	398.2	11.79	248.5	1.8
398.4	11.83	644.8	0.6	398.2	12.01	256.6	1.8
398.4	12.05	642.5	0.6	398.2	12.23	264.6	1.9
398.4	12.27	639.9	0.7	398.2	12.43	272.4	2.0
398.4	12.47	637.4	0.7	398.2	12.62	280.2	2.1
398.4	12.66	634.9	0.8	398.2	12.80	287.8	2.2
398.4	12.85	632.0	0.8	398.2	13.18	304.8	2.4
398.4	13.04	629.1	0.9	398.2	13.39	315.1	2.5
398.4	13.24	625.1	1.0	398.1	13.59	325.7	2.7
398.4	13.43	621.1	1.1	398.1	13.79	336.5	2.9
398.4	13.64	616.3	1.3	398.1	13.97	347.6	3.2
398.4	13.83	611.3	1.4	398.1	14.14	358.7	3.5
398.4	14.01	605.6	1.7	398.1	14.30	370.7	3.9
398.4	14.18	599.4	2.0	398.1	14.46	384.1	4.6
398.4	14.34	592.5	2.4	398.2	14.57	394.9	5.3
398.4	14.50	584.9	3.0	398.2	14.77	420.4	8.2
398.4	14.65	574.4	4.1	398.2	15.05	476.1	8.6
398.4	14.82	558.0	7.8	423.4	1.48	26.3	0.8
398.4	15.08	527.4	15.0	423.4	2.49	41.3	0.8
398.4	15.16	500.4	15.0	423.4	3.70	60.0	0.8
423.6	1.52	645.6	0.2	423.4	4.91	79.9	0.9
423.7	2.53	644.7	0.2	423.4	6.02	99.2	0.9
423.7	3.74	643.2	0.3	423.4	6.85	114.6	0.9
423.6	4.95	641.3	0.3	423.4	7.65	130.2	1.0
423.6	6.02	639.0	0.3	423.4	8.44	146.5	1.0
423.7	6.86	636.7	0.3	423.4	9.20	163.1	1.1
423.7	7.68	634.2	0.3	423.4	9.94	180.4	1.2
423.7	8.47	631.3	0.3	423.4	10.65	198.3	1.3
423.7	9.23	628.0	0.4	423.4	11.34	216.7	1.4
423.7	9.98	624.1	0.4	423.4	12.00	236.1	1.5
423.7	10.69	619.5	0.5	423.4	12.64	256.9	1.7
423.7	11.38	614.3	0.5	423.4	13.24	279.0	2.0
423.7	12.04	608.2	0.6	423.4	13.82	303.3	2.3
423.7	12.69	600.6	0.8	423.4	14.36	330.7	2.9
423.7	13.30	591.4	0.9	423.4	15.09	391.8	7.3
423.7	13.89	579.7	1.3	423.4	15.39	454.6	8.0
423.6	14.43	564.2	1.9	448.5	1.31	27.8	0.9
423.7	14.86	543.9	3.2	448.5	1.88	35.8	0.8
423.7	15.13	519.6	7.4	448.5	3.15	54.5	0.8
423.7	15.35	493.7	7.5	448.5	4.34	72.8	0.8

Table 2. continued

liquid phase				vapor phase			
T/K	p/MPa	$\rho/(kg \cdot m^{-3})$	$u(\rho)/(kg \cdot m^{-3})$	T/K	p/MPa	$\rho/(kg \cdot m^{-3})$	$u(\rho)/(kg \cdot m^{-3})$
423.7	15.44	475.5	7.5	448.5	4.63	77.6	0.8
448.7	1.34	617.2	0.3	448.5	4.66	76.3	0.8
448.8	1.91	616.1	0.3	448.5	5.70	95.3	0.9
448.8	3.19	613.8	0.3	448.5	6.67	112.4	0.9
448.8	4.37	611.0	0.3	448.5	7.54	128.8	0.9
448.8	4.67	610.2	0.3	448.5	8.40	145.7	1.0
448.8	4.68	610.1	0.3	448.5	9.24	163.5	1.1
448.8	5.68	607.2	0.3	448.5	10.07	182.4	1.2
448.8	6.67	603.8	0.3	448.5	10.87	202.2	1.3
448.8	7.55	600.2	0.4	448.5	11.63	223.1	1.4
448.8	8.41	596.0	0.4	448.5	12.39	246.5	1.7
448.8	9.26	591.2	0.4	448.5	13.12	272.8	2.0
448.8	10.09	585.4	0.5	448.5	13.82	304.7	2.8
448.8	10.90	578.5	0.6	448.5	14.48	357.4	6.7
448.8	11.68	570.4	0.7	448.5	13.25	272.0	2.1
448.8	12.45	560.1	0.8	448.5	13.97	313.4	3.2
448.8	13.19	546.7	1.1	448.5	14.01	317.1	3.3
448.8	13.89	527.4	1.8	448.5	14.29	336.5	4.5
448.8	14.03	523.4	2.0	448.5	14.57	372.9	9.2
448.8	14.32	508.9	3.0	448.5	14.87	425.8	9.3
448.8	14.55	490.9	5.8				
448.8	14.61	485.8	6.5				
448.8	14.92	445.4	6.5				

[a]Standard uncertainties in temperature, pressure, and period oscillation were $u(T)$ = 0.2 K, $u(p)$ = 0.05 MPa, and $u(\tau)$ = 0.01 μs, respectively. [b]Standard uncertainty of density is represented by $u(\rho)$.

operating in the pressure control mode, maintained the system pressure constant. The periods of oscillation, temperature, and pressure of the lower VTD were recorded over a period of 3 min. The measurement was considered acceptable when the standard deviation of the period of oscillation was less than 0.01 μs. A similar method was used to determine the vapor-phase density. The cell contents were remixed, and then, at constant pressure, 4 mL of the vapor phase was displaced into the top VTD, and the temperature, pressure, and period of oscillation were recorded. The pressure was then increased by injecting more CO_2 and a new measurement cycle was initiated; the procedure was repeated until the isotherm was completed. It should be noted that neither the vapor- nor the liquid-phase compositions can be measured within the present apparatus. Software written in Agilent VEE was created to automate the whole experimental method, enhancing measurement repeatability. Figure 1 shows the reproducibility of a data set at T = 373 K. Based on these experiments, we estimated that our repeatability uncertainty was about 1 kg·m^{-3}.

2.3. Calibration and Uncertainty. In the vibrating-tube densimeters, the density was calculated using the following working equation

$$\rho = \frac{(\rho_M/S_{00})}{(1 + \alpha_V t + \beta_V p)}\left(\left(\frac{\tau}{\tau_{00}(1 + \varepsilon_{\tau 1} t + \varepsilon_{\tau 2} t^2)}\right)^2 (1 + \beta_\tau p) - 1\right)$$

(1)

where p is the pressure, t is the Celsius temperature, and ρ_M is the density of the vibrating-tube material, which was Hastelloy (ρ_M = 8.89 g·cm^{-3}). S_{00}, α_V, β_V, τ_{00}, $\varepsilon_{\tau 1}$, $\varepsilon_{\tau 2}$, and β_τ are physical parameters of the vibrating-tube densimeter obtained using the calibration procedure described in our previous paper.[28,29] The two densimeters were calibrated under vacuum at all temper-

atures and with water across the whole temperature and pressure ranges. Since only water and vacuum were used in the calibration, the constraint, $\beta_\tau = (-\beta_V/3.87)$, was included in the adjustment. The densities of water were obtained from the IAPWS formulation,[30] as implemented in the REFPROP 10.0 database.[31] Figure 2 shows the deviation of the calibration for the top and bottom VTDs as an illustration.

The temperature sensors were calibrated on the ITS-90 in a triple-point-of-water cell and by comparison with a standard 25 Ω PRT submerged in a stirred oil bath over a temperature range of 313−473 K. The pressure transducers were calibrated against a reference quartz-crystal pressure gauge (Fluke, model PPCH-G 70 M) having a standard relative uncertainty of 0.014 MPa.[27] Taking into account the calibration uncertainty, the uniformity, and the stability of the oven, the estimated standard uncertainty of the measured temperature was 0.2 K. The standard uncertainty of the measured pressures was 0.05 MPa.

The overall standard uncertainty of the densities was calculated following the guidelines described in the GUM[33] and was estimated to be less than 1.5 kg·m^{-3} throughout most of the temperature and pressure ranges, except for measurements in the near-critical region where uncertainties of up to about 20 kg·m^{-3} are found. The experimental data and calculated uncertainties are given in Table 2.

3. RESULTS AND DISCUSSION

The bubble-point and dew-point densities of the (CO_2 + methylcyclohexane) system were measured up to just below the critical pressures on seven isotherms at temperatures from 298 to 448 K in intervals of 25 K and the results are plotted in Figure 3. The dew-point densities for all of the studied isotherms consistently increased with the pressure, whereas, at temperatures higher than 373 K, the bubble-point densities decreased
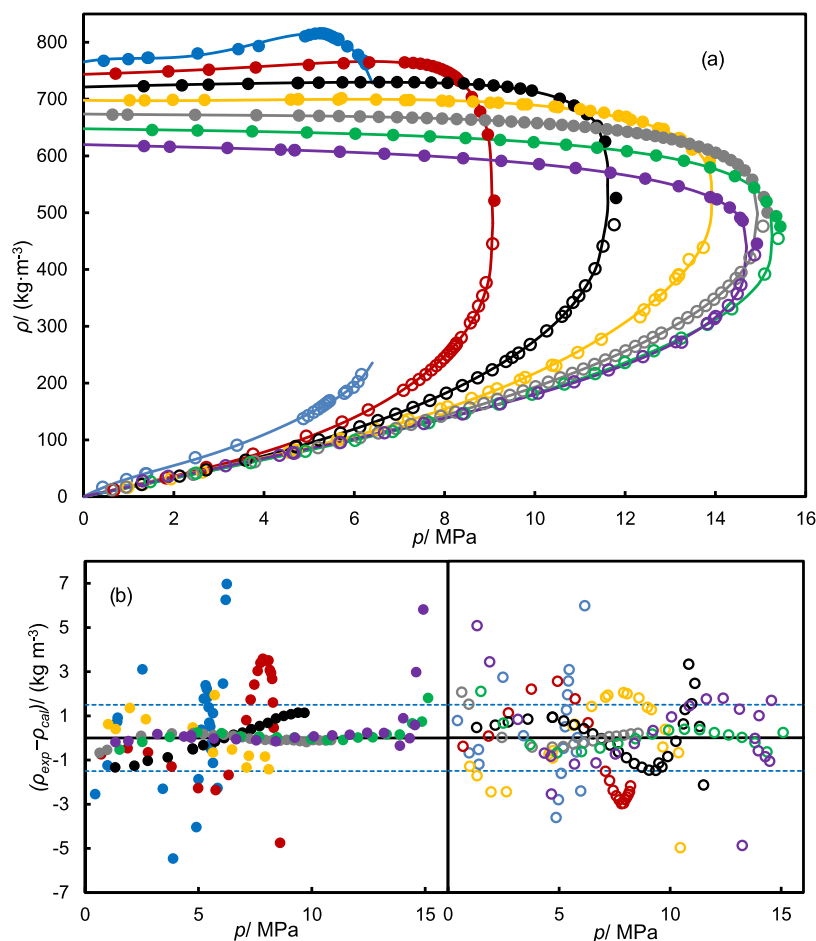
Figure 3. (a) Experimental saturated-phase densities ρ of the CO_2 + methylcyclohexane system versus pressure p at several temperatures. Colored continuous curves estimated from eq 2 with parameters from Table 3. (b) Deviations between the experimental densities and those calculated by eq 2. Dew-point densities (empty symbols) and bubble-point densities (full symbols). Colors denote different temperatures: 298 K (blue), 323 K (red), 348 K (black), 373 K (yellow), 398 K (gray), 423 K (green), and 448 K (purple). ▪▪▪▪▪▪, ± 1.5 kg·m^{-3}.

Table 3. Parameters A_i, B_i, C, D, ρ_c, and p_c of Eq 2 for Saturated-Phase Densities of the (CO_2 + Methylcyclohexane) System[a]

T/K	298[b]	323	348	373	398	423	448
A_1/MPa^{-1}	−161.5	−58.66	−16.64	33.88	14.09	11.73	8.671
A_2/MPa^{-2}	4.753	1.870	0.2420	−3.514	−1.174	−0.8455	−0.6738
A_3/MPa^{-3}	1.351	0	0	0.1204	0.03712	0.02816	0.02874
A_4/MPa^{-4}	−0.1059	0	0	0	0	0	0
C/MPa$^{-\beta}$	776.0	547.9	397.5	247.5	249.8	233.3	228.3
ρ_c/(kg m^{-3})	444.0	481.6	548.5	525.5	498.2	459.1	439.6
B_1/MPa^{-1}	42.65	−97.95	−42.93	−43.54	−28.17	−25.97	−12.41
B_2/MPa^{-2}	−55.10	7.580	2.318	2.087	0.9060	0.8904	0.2074
B_3/MPa^{-3}	11.06	−0.2817	−0.06563	−0.05469	−0.02004	−0.02404	−0.01171
B_4/MPa^{-4}	−0.7118	0	0	0	0	0	0
D/MPa$^{-\beta}$	95.21	124.7	−39.24	−1.642	−15.45	1.646	−35.29
p_c/MPa	6.74	9.07	11.61	13.92	14.93	15.26	14.69
$\Delta_{AAD,L}$/(kg·m^{-3})	2.2	2.3	1.9	1.9	0.9	2.7	0.6
$10^2\Delta_{AARD,L}$	0.3	0.30	1.1	0.29	0.16	0.5	0.12
$\Delta_{AAD,V}$/(kg·m^{-3})	1.4	2.2	1.0	2.0	0.21	0.4	1.5
$10^2\Delta_{AARD,V}$	1.6	1.3	0.6	1.8	0.7	0.7	1.2

^{a}ρ_c and p_c represent the critical density and pressure, respectively. The values of the average absolute deviation Δ_{AAD} and average absolute relative deviation Δ_{AARD} between the experimental densities and those calculated by eq 2. The subscripts L and V symbolize the liquid and vapor phases. ^{b}ρ_c and p_c at 298 K are empirical values.

with the pressure. At T < 373 K, the liquid phase densities at first increased with pressure until a maximum was reached, after which the values declined up to the critical point. This behavior, which was particularly noticeable at temperatures of 298−323 K, has been observed for other (CO_2 + hydrocarbon) binary systems[17,18] and is attributed to the influence of CO_2 dissolving
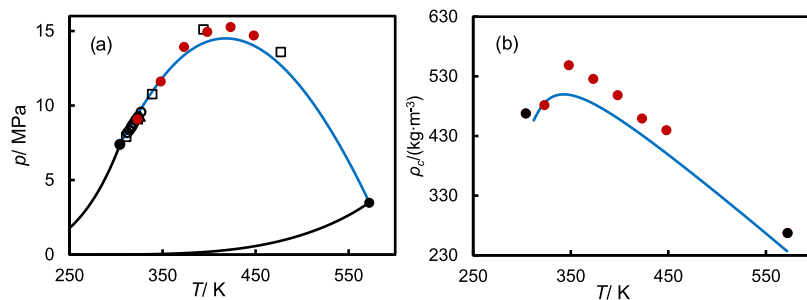
Figure 4. For the CO_2 + methylcyclohexane system, (a) critical pressure vs critical temperature: (red circle), this work from the saturated-phase densities; O, Zhang et al.;[26] □, Ng and Robinson;[22] Δ, Nasrifar et al.,[24] and the black line is the vapor pressure of the pure components obtained from the Helmholtz equation of state;[31,34] (b) critical density vs critical temperature; (red circle), this work from the saturated-phase densities. For (a, b), the blue line calculated using the procedure of Heidemann and Khalil[36] and the Peng−Robinson equation of state[23] with the van der Waals mixing rule (k_{ij} = 0) and ●, critical points of pure components.[31]
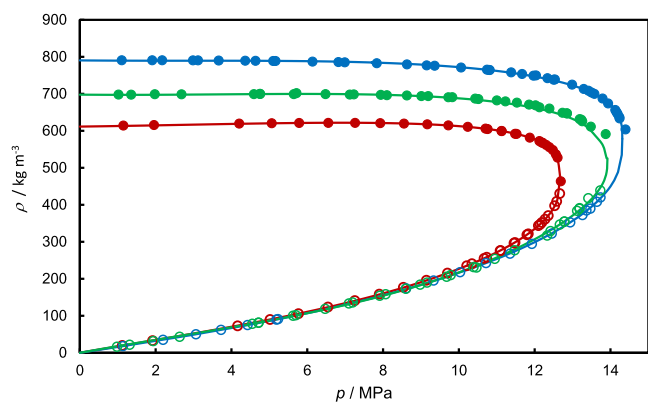
Figure 5. Experimental saturated-phase densities ρ versus pressures p at T = 373 K for (red circles) CO_2 + heptane;[18] (green circles) CO_2 + methylcyclohexane; and (blue circles) CO_2 + methylbenzene.[17] Dew-point densities (empty symbols) and bubble-point densities (full symbols). Colored continuous lines calculated from eq 2.

Table 4. Critical Temperature T_c, Critical Pressure p_c, and Acentric Factor ω for CO_2 and Methylcyclohexane[37]

component	T_c/K	p_c/MPa	ω
CO_2	304.16	7.381	0.2251
methylcyclohexane	572.31	3.482	0.2351

Table 5. Binary Interaction Parameter k_{12} in the PPR-78 EOS between CO_2 and Methylcyclohexane at Different Temperatures

T/K	k_{12}	T/K	k_{12}
298	0.1186	311	0.1168
323	0.1166	339	0.1172
348	0.1178	394	0.1224
373	0.1201	477	0.1330
398	0.1229		
423	0.1259		
448	0.1291		

in the liquid phase. A comparison between the mass densities of pure methylcyclohexane, calculated from the unpublished Helmholtz energy equation of state implemented in REFPROP 10.0,[32] and the mixture bubble-point densities revealed that the former was greater than the latter under the same conditions of temperatures and pressures, except for T = 298 K at p < 6 MPa
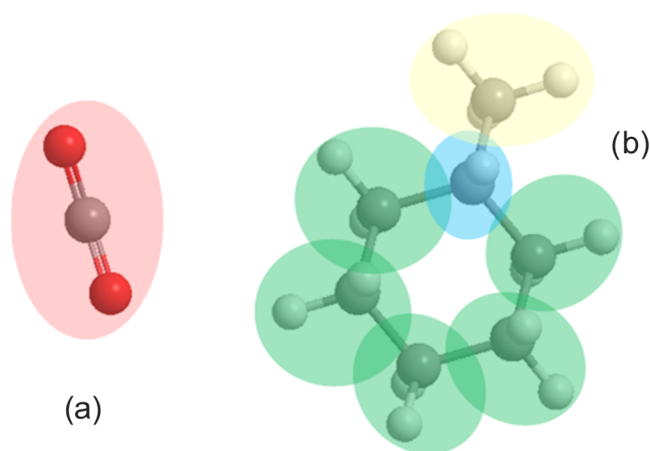
Figure 6. Model representation within the SAFT-γ Mie approach for the CO_2 + methylcyclohexane. (a) CO_2 is represented by a single group and (b) methylcyclohexane is represented with five cyclic methylene groups (cCH_2), one methyl group (cH_3), and one cyclic methine (cCH) group.

and T = 323 K at p < 8 MPa. In contrast, pure CO_2 densities[34] were consistently lower than the mixture dew-point densities.

The densities of bubble points and dew points were fitted isothermally using an empirical correlation of the following form

$$\left.\begin{aligned}
\rho_L - \rho_V &= \sum_{i=1}^{4} A_i(p_c - p)^i + C(p_c - p)^\beta \\
\rho_L + \rho_V &= 2\rho_c + \sum_{i=1}^{4} B_i(p_c - p)^i + D(p_c - p)^\beta
\end{aligned}\right\}$$

(2)

where p, ρ_L, and ρ_V are the experimental pressure, saturated liquid density, and saturated vapor density, respectively; p_c and ρ_c are the critical pressure and density, respectively; and β is a universal critical exponent taken to be 0.325. The terms in $(p_c - p)^\beta$ reflect the asymptotic scaling behavior of the coexisting vapor- and liquid-phase compositions in the approach to the critical pressure as the constant temperature.[35] To constrain the fitting at p = 0, the bubble-point density was set to the density of pure liquid methylcyclohexane at the same temperature extrapolated to zero pressure, using Helmholtz free-energy equation of state.[31] The dew-point density was set at 0. The Lenvenberg−Marquardt algorithm was used to minimize the sum of the squared differences between the experimental and calculated densities by manipulation of the adjustable

61

Table 6. Like Group Parameters Used in the SAFT-γ Mie Modeling[a]

group	ν_k^*	S_k	$\sigma_{kk}/$Å	λ_{kk}^r	λ_{kk}^a	$(\varepsilon_{kk}/k_B)/$K	references
CH$_3$	1	0.57255	4.0772	15.050	6	256.77	13
cCH$_2$	1	0.24751	4.7852	20.386	6	477.36	15
CO$_2$	2	0.8468	3.0500	26.408	5.055	207.89	14
cCH	1	0.0961	5.4116	8	6	699.92	45

[a]ν_k^* is the number of segments constituting a group, S_k is the shape factor, σ_{kk} is the size of group k, λ_{kk}^r is the repulsive exponent, λ_{kk}^a is the attractive exponent, and ε_{kk} is the Mie potential dispersion energy. k_B is Boltzmann's constant, $k_B = 1.380648813 \times 10^{-23}$ J K^{-1}.

Table 7. Unlike Group Cross Interaction Energies ε_{kl} Used the SAFT-γ Mie Modeling, Where k_B is Boltzmann's Constant[a]

group, k	group l	$(\varepsilon_{kl}/k_B)/$K	references
CH$_3$	cCH$_2$	355.95	15
CH$_3$	CO$_2$	205.70	15
CH$_3$	cCH	690.17	45
cCH$_2$	CO$_2$	269.68	16
cCH$_2$	cCH	321.71	45
CO$_2$	cCH	294.99	16

[a]The unlike attractive and repulsive exponents of the Mie potential, λ_{kl}^a and λ_{kl}^r, as well as the unlike distance and size parameters, r_{kl} and σ_{kl}, respectively, were obtained using combining rules described in eq 8.

parameters A_i, B_i, C, D, p_c, and ρ_c; the values obtained are given in Table 3. The absolute and relative average deviations (Δ_{AAD} and Δ_{AARD}) at each temperature are also given in Table 3. The experimental density deviations from the correlation are shown in Figure 3b. The Δ_{AAD} and Δ_{AARD} for the liquid phase were 1.7 kg·m^{-3} and 0.3%, whereas the same metrics for the vapor phase were 1.3 kg·m^{-3} and 1.2%, excluding the density data with experimental uncertainty higher than 10 kg·m^{-3}, that corresponded to data close to the critical point. These average deviations are quite similar to the experimental uncertainty, indicating that eq 2 provides a very good representation of the data. Table 3 gives the critical pressure and density determined by fitting the data at each temperature; however, the corresponding critical compositions are not determined. In Figure 4, the critical pressures obtained here are compared with those observed directly or estimated from VLE data in the literature[22,24,26,34] and it can be seen that these different data sets are in close agreement. In addition, Figure 4 shows the critical density obtained here versus the temperature and the critical curve calculated from the Peng−Robinson equation of state using the approach of Heidemann and Khalil.[23,36] In general, the Peng−Robinson model underestimated critical pressures and densities, but it followed the trajectory of the critical points.

Figure 5 shows the saturated-phase densities at $T = 373$ K for the three systems investigated in our current and previous work: CO$_2$ + heptane,[18] CO$_2$ + methylcyclohexane, and CO$_2$ + methylbenzene.[17] It can be seen that the dew-point densities for the three mixtures are very similar at low pressures but they start to differ as the critical point is approached. On the other hand, the bubble-point densities were ordered as follows: $\rho_{(CO_2+heptane)} < \rho_{(CO_2+methylcyclohexane)} < \rho_{(CO_2+methylbenzene)}$, as expected based on the densities of the pure hydrocarbon liquids.

In this work, both new experimental saturated-phase densities and VLE data from the literature are compared with two group-contribution models: the Predictive Peng−Robinson equation of state (PPR-78)[8] and a predictive version of the statistical associating fluid theory incorporating the Mie potential (SAFT-γ Mie).[13] These comparisons involve no parameter fitting as the models to be tested are purely predictive in the present context.

In the PPR-78 model, the Peng−Robinson equation of state is used

$$p(T, v) = \frac{RT}{v - b} - \frac{a(T)}{v(v + b) + b(v-b)} \tag{3}$$

where v is the molar volume, a is the attractive energy parameter, and b is the co-volume parameter. The following equations are used to calculate these parameters for individual components

$$
\left.
\begin{aligned}
a_i &= 0.457236(R^2 T_{c,i}^2/p_{c,i})\alpha_i(T) \\
\alpha_i(T) &= [1 + m_i(1 - \sqrt{T/T_{c,i}})]^2 \\
\omega_i &\leq 0.491 \quad m_i = 0.37464 + 1.54226\omega_i - 0.26992\omega_i^2 \\
\omega_i &> 0.491 \quad m_i = 0.379642 + 1.48503\omega_i - 0.164423\omega_i^2 + 0.01666\omega_i^3 \\
b_i &= 0.077796(RT_{c,i}/p_{c,i})
\end{aligned}
\right\} \tag{4}
$$

In eq 4, $T_{c,i}$, $p_{c,i}$, and ω_i are the critical temperature, critical pressure, and acentric factor of component i. The critical parameters and acentric factor were obtained from the NIST ThermoData Engine Version 10.1,[37] implemented in Aspen Properties version 9[38] and are shown in Table 4.

The Peng−Robinson EoS is usually applied to mixtures using the standard van der Waals mixing rule that is given as

$$
\left.
\begin{aligned}
a &= \sum_{i=1}^{N} \sum_{j=1}^{N} x_i x_j [1 - k_{ij}(T)]\sqrt{a_i a_j} \\
b &= \sum_{i=1}^{N} x_i b_i
\end{aligned}
\right\} \tag{5}
$$

where $k_{ij}(T) = k_{ji}(T)$ is the binary interaction parameter between components i and j and x_i is the mole fraction of component i. The group-contribution method developed by Jaubert and co-workers[8−10,39] was used to compute the temperature-dependent binary interaction between each pair of components. In this approach, the binary interaction parameter k_{ij} is given by

$$
k_{ij}(T) = \left[\left\{ -\frac{1}{2} \sum_{k=1}^{N_g} \sum_{l=1}^{N_g} (\alpha_{ik} - \alpha_{jk})(\alpha_{il} - \alpha_{ji}) \right. \right.
$$
$$
\left. A_{kl}(T_0/T)^{(B_{kl}/A_{kl}-1)} \right\} - \left\{ \frac{\sqrt{a_i(T)}}{b_i} - \frac{\sqrt{a_j(T)}}{b_j} \right\}^2 \right]
$$
$$
\left[\frac{2\sqrt{a_i(T)a_j(T)}}{b_i b_j} \right]^{-1} \tag{6}
$$
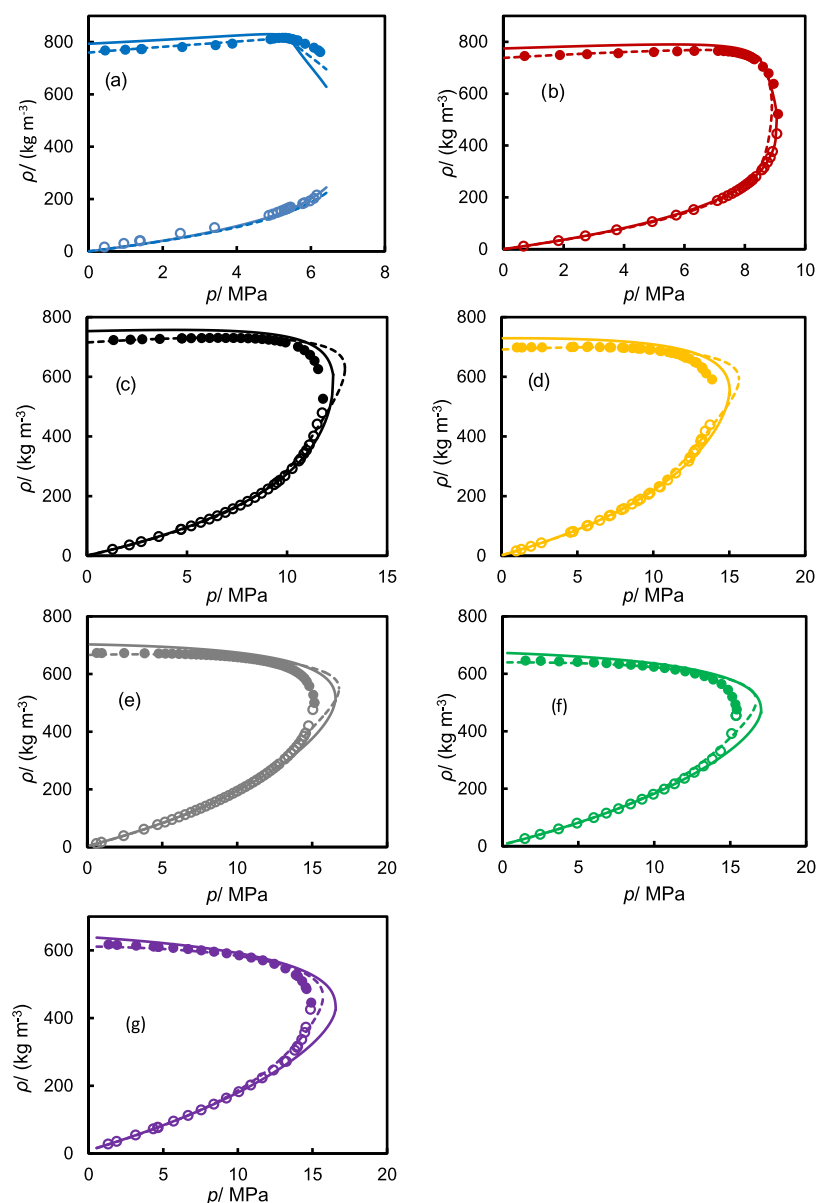
Figure 7. Experimental dew-point (open symbols) and bubble-point (filled symbols) densities and predictions from PPR-78 EoS (solid lines) and SAFT-γ Mie (dashed lines) at different temperatures: 298 K (a), 323 K (b), 348 K (c), 373 K (d), 398 K (e), 423 K (f), and 448 K (g) for the CO_2 + methylcyclohexane system.

where N_g is the number of distinct functional groups present in the system, α_{ik} is the occurrence of group k in molecule i divided by the total number of groups present in that component, and A_{kl} and B_{kl} are group parameters. Jaubert and co-workers obtained tables of the group parameters by fitting to an extensive database of experimental binary VLE data.[10] The binary interaction parameter k_{ij} calculated from eq 6 and used in this work is listed in Table 5. The vapor–liquid equilibrium and density calculations with the PPR-78 model were carried out in the Aspen Properties package software version 9.[38]

In SAFT-γ Mie, the molecules are represented as (possibly associating) heteronuclear chains of fused spherical segments that interact according to the Mie potential,[13−16,40] defined as follows

$$u_{kl}(r_{kl}) = \left(\frac{\lambda_{kl}^r \varepsilon_{kl}}{\lambda_{kl}^r - \lambda_{kl}^a}\right)\left(\frac{\lambda_{kl}^r}{\lambda_{kl}^a}\right)^{\lambda_{kl}^a/(\lambda_{kl}^r - \lambda_{kl}^a)}\left[\left(\frac{\sigma_{kl}}{r_{kl}}\right)^{\lambda_{kl}^r} - \left(\frac{\sigma_{kl}}{r_{kl}}\right)^{\lambda_{kl}^a}\right]$$

(7)

where u_{kl} is the potential energy of interaction between segments k and l that represent functional groups in the molecule. The repulsive and attractive exponents are λ_{kl}^r and λ_{kl}^a, respectively; the energy parameter is ε_{kl}, the distance between the two groups is r_{kl}, and the size parameter is σ_{kl}. An additional parameter, the shape factor, S_k, determines the extent to which functional group k contributes to the molecule properties. The parameters that characterize the interactions between identical functional groups, known as like parameters and including the shape factor, are estimated by regression to experimental data, such as vapor pressures and compress-liquid densities, of a series of compounds that contain that group.[13] The parameters that define the interactions between different functional groups,
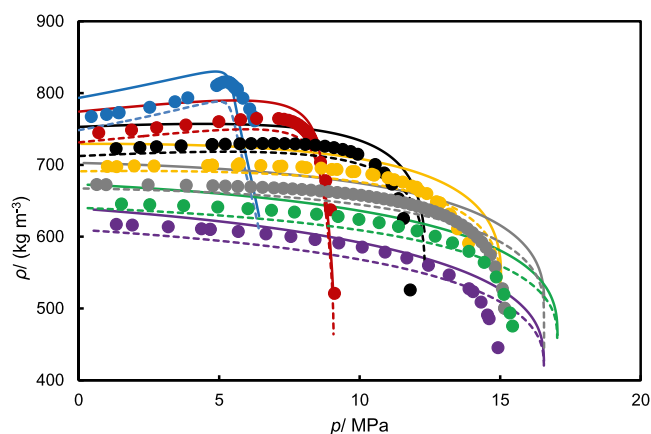
Figure 8. Experimental bubble-point densities (symbols) and predictions from PPR-78 without volume translation (solid line) and with Peneloux volume translation (dashed line). Colors symbolize different temperatures: 298 K (blue), 323 K (red), 348 K (black), 373 K (yellow), 398 K (gray), 423 K (green), and 448 K (purple).
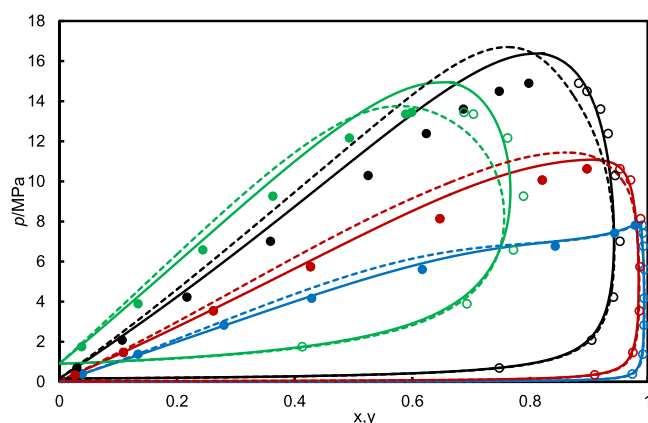
Figure 9. Bubble-point (complete symbol) and dew-point (empty symbol) pressures p versus CO_2 mole fraction (x, y) for CO_2 + methylcyclohexane at (blue) 311 K, (red) 339 K, (black) 394 K, and (green) 477 K. The symbols represent the experimental data published by Ng and Robinson,[22] the dashed lines are the prediction of the SAFT-γ Mie model, and the continuous lines are the prediction of the PPR-78 equation of state.

known as unlike parameters, can be estimated using combining rules or else obtained by regression against experimental data for pure substances or binary mixtures. Small molecules, such as CO_2, are each represented by a single group. On the other hand, methylcyclohexane is represented by three functional groups: cyclic CH_2, cyclic CH, and CH_3. The SAFT-γ Mie molecular models for the CO_2 + methylcyclohexane system are illustrated in Figure 6. Tables 6 and 7 give the values and literature sources of the parameters utilized for the individual groups. The following combining rules were used to determine the unlike parameters that are not listed in Table 7

$$\sigma_{kl} = \frac{1}{2}(\sigma_{kk} + \sigma_{ll})$$

$$r_{kl} = \frac{1}{2}(r_{kk} + r_{ll})$$

$$\varepsilon_{kl} = \frac{\sqrt{\sigma_{kk}^3 \sigma_{ll}^3}}{\sigma_{kl}^3}\sqrt{\varepsilon_{kk}\varepsilon_{ll}}$$

$$\lambda_{kl} = 3 + \sqrt{(\lambda_{kk}-3)(\lambda_{ll}-3)} \tag{8}$$

The calculations of SAFT-γ Mie predictions were carried out in gPROMS software developed by PSE Ltd.[41]

Figure 7 illustrates the saturated-phase density predictions obtained from the PPR-78 and SAFT-γ Mie models. It should be noted that for both models, experimental data closer than 0.9 pc were excluded from the calculation of Δ_{AAD}. The dew-point densities predicted by PPR-78 are mostly in excellent agreement with the experimental data with $\Delta_{AADV} = 3$ kg·m^{-3}. However, the bubble-point densities are overpredicted with $\Delta_{AADL} = 20$ kg·m^{-3}. This behavior is expected as cubic equations are known to offer relatively poor accuracy for liquid densities. To minimize the deviation between the experimental and predicated bubble-point densities, the Peneloux volume translation function,[42] with the volume corrections calculated from the Rackett compressibility factor, was incorporated in the PPR-78 model. Figure 8 shows the densities calculated from the PPR-78 model with and without the inclusion of volume translation. As shown in Figure 8, including volume translation in the model improves the predictions with $\Delta_{AADL} = 14$ kg·m^{-3}.[43] Figure 7 shows that SAFT-γ Mie provides rather accurate predictions of the saturated vapor-phase and liquid-phase densities across the full range of conditions studied with $\Delta_{AADV} = 6$ kg·m^{-3} for the vapor-saturated densities and $\Delta_{AADL} = 4$ kg·m^{-3} for the liquid-saturated densities. Both models generally overpredict the critical pressure, leading to poor predictions around the critical region, except at $T = 323$ K.

To evaluate the predictive capabilities of PPR-78 and SAFT-γ Mie for the coexisting phase compositions of the CO_2 + methylcyclohexane system, the bubble- and dew-point data reported by Ng and Robinson[22] were selected. This data was considered in particular because they pertain to the temperature range studied here and include both dew and bubble points. Figure 9 shows generally good agreement for dew-point data with both models. The Δ_{AADV} for the mole fraction of CO_2 was 0.014 and 0.011 for PPR-78 and SAFT-γ Mie, respectively. However, bubble points are predicted less accurately with Δ_{AADL} = 0.026 for PPR-78 and Δ_{AADL} = 0.046 for SAFT-γ Mie. As it can be inferred, the PPR-78 generally performs better than SAFT-γ Mie for bubble-point compositions. This may be because VLE data for the (CO_2 + methylcyclohexane) system were regressed in the determination of the PPR-78 group parameters,[44] whereas in the SAFT-γ Mie, the unlike dispersion energy parameters between CO_2 and the cyclic CH_2 have been obtained only using CO_2 + cyclohexane and CO_2 + cyclopentane systems.[45,46] Although the authors[46] indeed used CO_2 + methylcyclohexane for the calculation ε_{kl} of CO_2 and the cyclic CH. Again, one can observe overprediction of the critical pressure for both models.

4. CONCLUSIONS

For the first time, experimental saturated-phase densities for the (CO_2 + methylcyclohexane) system are reported over an extended temperature range with pressures up to the critical.

Except for a few measurements in the critical region, the estimated standard uncertainty is less than 1.5 kg·m^{-3}. An empirical correlation was used to fit the densities with Δ_{AAD} = 1.5 kg·m^{-3}, allowing interpolation of the data along isotherms as well as the determination of critical pressures and densities. The predictive capacity of two equations of states, PPR-78 and SAFT-γ Mie, was evaluated against our saturated-phase densities and VLE data from the literature. At the studied conditions, both models predicted dew-point pressures and densities reasonably well. Neither model was correct in the critical region except, perhaps fortuitously, at T = 323 K. In predicting saturated liquid densities, SAFT-γ Mie performed better than PPR-78, even when volume translation was included in the latter, whereas the opposite was true for bubble-point pressures. This might imply that certain unlike parameters in SAFT-γ Mie could be optimized further against VLE data.

■ AUTHOR INFORMATION

Corresponding Author

Yolanda Sanchez-Vicente − *Qatar Carbonates and Carbon Storage Research Centre (QCCSRC), Department of Chemical Engineering, Imperial College London, London SW7 2AZ, United Kingdom; Department of Mechanical & Construction Engineering, Faculty of Engineering and Environment, Northumbria University, Newcastle upon Tyne NE1 8ST, United Kingdom;* ⦿ orcid.org/0000-0002-8221-7646; Email: yolanda.vicente@northumbria.ac.uk

Author

J. P. Martin Trusler − *Qatar Carbonates and Carbon Storage Research Centre (QCCSRC), Department of Chemical Engineering, Imperial College London, London SW7 2AZ, United Kingdom;* ⦿ orcid.org/0000-0002-6403-2488

Complete contact information is available at:
https://pubs.acs.org/10.1021/acs.jced.1c00718

Notes

The authors declare no competing financial interest.

■ ACKNOWLEDGMENTS

■ REFERENCES

(1) McHugh, M. A.; Krukonis, V. J. *Supercritical Fluid Extraction Principles and Practice*; Elsevier, 1994.

(2) Li, Q.; Feng, Z.; Rangaiah, G. P.; Dong, L. Process Optimization of Heat-Integrated Extractive Dividing-Wall Columns for Energy-Saving Separation of CO$_2$ and Hydrocarbons. *Ind. Eng. Chem. Res.* **2020**, *59*, 11000−11011.

(3) Sánchez-Vicente, Y.; Stevens, L.; Pando, C.; Cabañas, A. Functionalization of Silica SBA-15 with [3-(2-Aminoethylamino)-Propyl] Trimethoxysilane in Supercritical CO$_2$ Modified with Methanol or Ethanol for Carbon Capture. *Energies* **2020**, *13*, No. 5804.

(4) Koh, C. A.; Sloan, E. D.; Sum, A. K.; Wu, D. T. Fundamentals and Applications of Gas Hydrates. *Annu. Rev. Chem. Biomol. Eng.* **2011**, *2*, 237−257.

(5) Bui, M.; Adjiman, C. S.; Bardow, A.; Anthony, E. J.; Boston, A.; Brown, S.; Fennell, P. S.; Fuss, S.; Galindo, A.; Hackett, L. A.; Hallett, J. P.; Herzog, H. J.; Jackson, G.; Kemper, J.; Krevor, S.; Maitland, G. C.; Matuszewski, M.; Metcalfe, I. S.; Petit, C.; Puxty, G.; Reimer, J.; Reiner, D. M.; Rubin, E. S.; Scott, S. A.; Shah, N.; Smit, B.; Trusler, J. P. M.; Webley, P.; Wilcox, J.; Mac Dowell, N. Carbon capture and storage (CCS): the way forward. *Energy Environ. Sci.* **2018**, *11*, 1062−1176.

(6) Kontogeorgis, G. M.; Dohrn, R.; Economou, I. G.; de Hemptinne, J.-C.; ten Kate, A.; Kuitunen, S.; Mooijer, M.; Žilnik, L. F.; Vesovic, V. Industrial Requirements for Thermodynamic and Transport Properties: 2020. *Ind. Eng. Chem. Res.* **2021**, *60*, 4987−5013.

(7) Bouzalakos, S.; Maroto-Valer, M. M.; Ogden, J.; Johnson, N.; de Coninck, H.; de Best-Waldhober, M.; Groenenberg, H.; Elkamel, A.; Mirzaesmaeeli, H.; Croiset, E.; Douglas, P. L.; Desideri, U.; Davidson, R. M.; Basile, A.; Iulianelli, A.; Gallucci, F.; Morrone, P.; Higman, C.; Mathieu, P.; Kluiters, S. C.; van den Brink, R. W.; Haije, W. G.; Anthony, E. J.; Aspelund, A.; Seevam, P. N.; Race, J. M.; Downie, M. J.; Solomon, S.; Flach, T.; Ghoshal, S.; Zeman, F.; Birat, J.-P. Contributor Contact Details. In *Developments and Innovation in Carbon Dioxide (CO2) Capture and Storage Technology*; Maroto-Valer, M. M., Ed.; Woodhead Publishing, 2010; Vol. *1*, pp xiii−xvi.

(8) Jaubert, J.-N.; Mutelet, F. VLE predictions with the Peng−Robinson equation of state and temperature dependent kij calculated through a group contribution method. *Fluid Phase Equilib.* **2004**, *224*, 285−304.

(9) Jaubert, J.-N.; Privat, R. Relationship between the binary interaction parameters (kij) of the Peng−Robinson and those of the Soave−Redlich−Kwong equations of state: Application to the definition of the PR2SRK model. *Fluid Phase Equilib.* **2010**, *295*, 26−37.

(10) Vitu, S.; Privat, R.; Jaubert, J. N.; Mutelet, F. Predicting the phase equilibria of CO$_2$+ hydrocarbon systems with the PPR78 model (PR EOS and k$_{ij}$ calculated through a group contribution method). *J. Supercrit. Fluids* **2008**, *45*, 1−26.

(11) Vitu, S.; Jaubert, J.-N.; Mutelet, F. Extension of the PPR78 model (Predictive 1978, Peng−Robinson EOS with temperature dependent kij calculated through a group contribution method) to systems containing naphtenic compounds. *Fluid Phase Equilib.* **2006**, *243*, 9−28.

(12) Al Ghafri, S. Z.; Maitland, G. C.; Trusler, J. P. M. Experimental and modeling study of the phase behavior of synthetic crude oil+CO$_2$. *Fluid Phase Equilib.* **2014**, *365*, 20−40.

(13) Papaioannou, V.; Lafitte, T.; Avendano, C.; Adjiman, C. S.; Jackson, G.; Muller, E. A.; Galindo, A. Group contribution methodology based on the statistical associating fluid theory for heteronuclear molecules formed from Mie segments. *J. Chem. Phys.* **2014**, *140*, No. 054107.

(14) Papaioannou, V.; Calado, F.; Lafitte, T.; Dufal, S.; Sadeqzadeh, M.; Jackson, G.; Adjiman, C. S.; Galindo, A. Application of the SAFT-gamma Mie group contribution equation of state to fluids of relevance to the oil and gas industry. *Fluid Phase Equilib.* **2016**, *416*, 104−119.

(15) Dufal, S.; Papaioannou, V.; Sadeqzadeh, M.; Pogiatzis, T.; Chremos, A.; Adjiman, C. S.; Jackson, G.; Galindo, A. Prediction of Thermodynamic Properties and Phase Behavior of Fluids and Mixtures with the SAFT-gamma Mie Group-Contribution Equation of State. *J. Chem. Eng. Data* **2014**, *59*, 3272−3288.
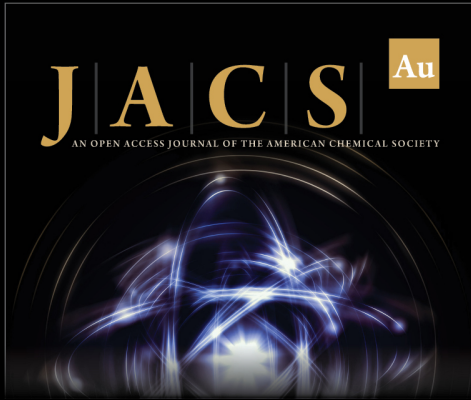
(16) Haslam, A. J.; Gonzalez-Perez, A.; Di Lecce, S.; Khalit, S. H.; Perdomo, F. A.; Kournopoulos, S.; Kohns, M.; Lindeboom, T.; Wehbe, M.; Febra, S.; Jackson, G.; Adjiman, C. S.; Galindo, A. Expanding the Applications of the SAFT-gamma Mie Group-Contribution Equation of State: Prediction of Thermodynamic Properties and Phase Behavior of Mixtures. *J. Chem. Eng. Data* **2020**, *65*, 5862−5890.

(17) Sanchez-Vicente, Y.; Tay, W. J.; Al Ghafri, S. Z.; Efika, E. C.; Trusler, J. P. M. Density and Phase Behavior of the CO$_2$ + Methylbenzene System in Wide Ranges of Temperatures and Pressures. *Ind. Eng. Chem. Res.* **2020**, *59*, 7224−7237.

(18) Sanchez-Vicente, Y.; Tay, W. J.; Al Ghafri, S. Z.; Trusler, J. P. M. Thermodynamics of carbon dioxide-hydrocarbon systems. *Appl. Energy* **2018**, *220*, 629−642.

(19) Al Ghafri, S. Z. S.; Trusler, J. P. M. Phase equilibria of (Methylbenzene + Carbon dioxide + Methane) at elevated pressure: Experiment and modelling. *J. Supercrit. Fluids* **2019**, *145*, 1−9.

(20) Al Ghafri, S. Z. S.; Maitland, G. C.; Trusler, J. P. M. Phase Behavior of the System (Carbon Dioxide + n-Heptane + Methylbenzene): A Comparison between Experimental Data and SAFT-γ-Mie Predictions. *J. Chem. Eng. Data* **2017**, *62*, 2826−2836.

(21) Field, L. R.; Wilhelm, E.; Battino, R. The solubility of gases in liquids 6. Solubility of N_2, O_2, CO, CO_2, CH_4, and CF_4 in methylcyclohexane and toluene at 283 to 313 K. *J. Chem. Thermodyn.* **1974**, *6*, 237−243.

(22) Ng, H.-J.; Robinson, D. B. The equilibrium phase properties of selected naphthenic binary systems: Carbon dioxide-methylcyclohexane, hydrogen sulfide-methylcyclohexane. *Fluid Phase Equilib.* **1979**, *2*, 283−292.

(23) Peng, D.; Robinson, D. B. A New Two-Constant Equation of State. *Ind. Eng. Chem. Fundam.* **1976**, *15*, 59−64.

(24) Nasrifar, K.; Mooijer-van den Heuvel, M. M.; Peters, C. J.; Ayatollahi, S.; Moshfeghian, M. Measurements and modeling of bubble points in binary carbon dioxide systems with tetrahydropyran and methylcyclohexane. *Fluid Phase Equilib.* **2003**, *204*, 1−14.

(25) Mota-Martinez, M. T.; Samdani, S.; Berrouk, A. S.; Rocha, M. A. A.; Alhseinat, E. Y.; Banat, F.; Kroon, M. C.; Peters, C. J. Design and test of a new high pressure phase equilibrium apparatus for highly corrosive mixtures of importance for natural gas. *J. Nat. Gas Sci. Eng.* **2015**, *27*, 661−665.

(26) Zhang, H. F.; Han, B. X.; Hou, Z. S.; Liu, Z. M. Measurement of critical points of the methylcyclohexane (MCH)-H_2-CO_2 system in the CO_2-rich region. *Fluid Phase Equilib.* **2001**, *179*, 131−138.

(27) Efika, E. C.; Hoballah, R.; Li, X.; May, E. F.; Nania, M.; Sanchez-Vicente, Y.; Trusler, J. P. M. Saturated phase densities of (CO_2 + H_2O) at temperatures from (293 to 450) K and pressures up to 64 MPa. *J. Chem. Thermodyn.* **2016**, *93*, 347−359.

(28) May, E. F.; Tay, W. J.; Nania, M.; Aleji, A.; Al-Ghafri, S.; Trusler, J. P. M. Erratum: "Physical apparatus parameters and model for vibrating tube densimeters at pressures to 140 MPa and temperatures to 473 K" [Rev. Sci. Instrum. 85, 095111 (2014)]. *Rev. Sci. Instrum.* **2015**, *86*, No. 049902.

(29) May, E. F.; Tay, W. J.; Nania, M.; Aleji, A.; Al-Ghafri, S.; Trusler, J. P. M. Physical apparatus parameters and model for vibrating tube densimeters at pressures to 140 MPa and temperatures to 473 K. *Rev. Sci. Instrum.* **2014**, *85*, No. 095111.

(30) Wagner, W.; Pruß, A. The IAPWS Formulation 1995 for the Thermodynamic Properties of Ordinary Water Substance for General and Scientific Use. *J. Phys. Chem. Ref. Data* **2002**, *31*, 387−535.

(31) Lemmon, E. W.; Bell, I. H.; Huber, M. L.; McLinden, M. O.. *NIST Standard Reference Database 23: Reference Fluid Thermodynamic and Transport Properties-REFPROP*, Version 10; Gaithersburg, 2018.

(32) Linstrom, P. J.; Mallard, W. G. *NIST Chemistry WebBook*; NIST Standard Reference Database Number 69; National Institute of Standards and Technology: Gaithersburg, MD, 2016. http://webbook.nist.gov (retrieved July 19, 2016).

(33) JCGM 100:2008. *Evaluation of Measurement Data − Guide to the Expression of Uncertainty in Measurement*; Joint Committee for Guides in Metrology, 2008.

(34) Span, R.; Wagner, W. A New Equation of State for Carbon Dioxide Covering the Fluid Region from the Triple-Point Temperature to 1100 K at Pressures up to 800 MPa. *J. Phys. Chem. Ref. Data* **1996**, *25*, 1509−1596.

(35) Niesen, V. G.; Rainwater, J. C. Critical locus, (vapor + liquid) equilibria, and coexisting densities of (carbon dioxide + propane) at temperatures from 311 K to 361 K. *J. Chem. Thermodyn.* **1990**, *22*, 777−795.

(36) Heidemann, R. A.; Khalil, A. M. The calculation of critical points. *AIChE J.* **1980**, *26*, 769−779.

(37) Diky, V.; Muzny, C.; Smolyanitsky, A.; Bazyleva, A.; Chirico, R.; Magee, J.; Paulechka, Y.; Kazakov, A.; Townsend, S.; Lemmon, E.; Frenkel, M.; Kroenlein, K. *ThermoData Engine (TDE) Version 10.1 (Pure Compounds, Binary Mixtures, Ternary Mixtures, and Chemical Reactions): NIST Standard Reference Database 103b*; National Institute of Standards and Technology: Gaithersburg, MD, 2016.

(38) Aspen Technology. *Aspen Properties*. v9; 2016.

(39) Xu, X.; Jaubert, J.-N.; Privat, R.; Arpentinier, P. Prediction of Thermodynamic Properties of Alkyne-Containing Mixtures with the E-PPR78 Model. *Ind. Eng. Chem. Res.* **2017**, *56*, 8143−8157.

(40) Dufal, S.; Lafitte, T.; Haslam, A. J.; Galindo, A.; Clark, G. N. I.; Vega, C.; Jackson, G. The A in SAFT: developing the contribution of association to the Helmholtz free energy within a Wertheim TPT1 treatment of generic Mie fluids. *Mol. Phys.* **2015**, *113*, 948−984.

(41) PSE Ltd. *gPROMS* V.7.0.7, 2021. http://www.psenterprise.com.

(42) Péneloux, A.; Rauzy, E.; Fréze, R. A consistent correction for Redlich-Kwong-Soave volumes. *Fluid Phase Equilib.* **1982**, *8*, 7−23.

(43) Privat, R.; Jaubert, J.-N.; Le Guennec, Y. Incorporation of a volume translation in an equation of state for fluid mixtures: which combining rule? which effect on properties of mixing? *Fluid Phase Equilib.* **2016**, *427*, 414−420.

(44) Vitu, S.; Privat, R.; Jaubert, J.-N.; Mutelet, F. Predicting the phase equilibria of CO2+hydrocarbon systems with the PPR78 model (PR EOS and kij calculated through a group contribution method). *J. Supercrit. Fluids* **2008**, *45*, 1−26.

(45) Perdomo, F. A.; Khalit, S. H.; Adjiman, C. S.; Galindo, A.; Jackson, G. Description of the thermodynamic properties and fluid-phase behavior of aqueous solutions of linear, branched, and cyclic amines. *AIChE J.* **2021**, *67*, No. e17194.

(46) Perdomo, F. A.; Khalit, S. H.; Graham, E. J.; Tzirakis, F.; Tsivintzelis, I.; Papadopoulos, A. I.; Seferlis, P.; Galindo, A.; Jackson, G.; Adjiman, C. S. Thermodynamic modelling of CO_2 absorption in cyclicamines, alkanolamines and phase-change amines using the SAFT-γ Mie group contribution approach.